Carbon 134 (2018) 92–102

Contents lists available at ScienceDirect

Carbon

journal homepage: www.elsevier.com/locate/carbon

Cellulose nanocrystals effect on the stabilization of polyacrylonitrile composite films

Jeffrey Luo [a, b], Huibin Chang [a, b], Po-Hsiang Wang [a], Robert J. Moon [a, b, c], Satish Kumar [a, b, *]

[a] School of Materials Science and Engineering, Georgia Institute of Technology, Atlanta, GA, 30332, USA
[b] Renewable Bioproducts Institute, Georgia Institute of Technology, Atlanta, GA, USA
[c] The Forest Products Laboratory, US Forest Service, Madison, WI, 53726, USA

ARTICLE INFO

Article history:
Received 2 November 2017
Received in revised form
16 February 2018
Accepted 24 March 2018
Available online 26 March 2018

ABSTRACT

The stabilization kinetics of polyacrylonitrile-co-methacrylic acid (PAN-co-MAA) and cellulose nanocrystal (CNC) composite films were studied with up to 40 wt% CNC loading using differential scanning calorimetry (DSC). It was determined that the addition of CNC reduced the activation energy of the polyacrylonitrile cyclization reaction by 16% irrespective of the CNC loading in the range of 5–40 wt%. There was also a development of a new exothermic peak in the PAN-co-MAA/CNC composite films after cyclization not seen in the neat PAN-co-MAA and neat CNC samples, indicating a different set of reactions occurring. Fourier transform infrared spectroscopy (FTIR) and wide-angle X-ray diffraction (WAXD) demonstrated that CNC within the PAN-co-MAA/CNC composite films were more thermally stable than the neat CNC film. Additionally, for the composite films, their reaction rate constants for cyclization and oxidations were found to be higher than neat PAN-co-MAA at certain temperatures, indicating that the addition of CNC into PAN-co-MAA can reduce the energy needed for stabilization.

1. Introduction

Carbon materials such as carbon fiber and carbon films have growing market demand due to their unique set of properties such as high mechanical, electrical, and thermal properties. Polyacrylonitrile (PAN) is the main precursor for carbon fiber, and there have been many previous studies on the stabilization of PAN fibers dating back to the 1950s [1–9], though there have not been many studies on the stabilization of PAN films [10,11]. The stabilization reactions in PAN include cyclization, dehydrogenation, oxidation, and crosslinking [2,12,13]. There have also been many thermal and carbonization studies of cellulose [14–17]. The stabilization and carbonization reactions of cellulose include dehydration, depolymerization, and aromatization [16,18].

With cellulose being the world's most abundant biopolymer in the world it is a resource of interest for the production of carbon fiber and carbon material. There have been recent efforts to reduce the cost of carbon fiber and to make carbon fiber from more environmentally sustainable materials such as cellulose and lignin [3,19–22]. Cellulose and lignin have prior history in being made into carbon fiber. Thomas Edison carbonized natural fibers to make carbon fibers for the filament in incandescent light bulbs in the 1800s [23]. Previously in the 1960s and 1970s there was a lignin based carbon fiber (Kayacarbon) produced at Nippon Kayaku Co. on a pilot scale. Lignin based carbon fiber had low tensile strength (~0.3 GPa), and is no longer commercially available [24,25]. Rayon, a cellulose based fiber, is also another fiber that is used to make carbon fiber and rayon based carbon fiber is still being produced by a Belarus based company SvetlogorskKhimvolokno [12,24].

A new class of cellulose base nano-sized particle, cellulose nanocrystals (CNC), may offer new opportunities to make carbon fibers more renewable and cheaper. CNC are biodegradable and renewable rod-like particles (diameter of 3–20 nm and a length of 50–500 nm) having high surface area, low toxicity, and surface chemistry that can be readily modified [26–28]. Studies investigating the effects of CNC additions to PAN based polymers have shown that high loading of CNCs, and good dispersions can be achieved in PAN [29–31].

This study investigates the reaction kinetics of stabilization of PAN-co-MAA/CNC composites. The knowledge gained helps in the

* Corresponding author. School of Materials Science and Engineering, Georgia Institute of Technology, 801 Ferst Dr, Atlanta, GA, 30332-0295, USA.
E-mail address: satish.kumar@gatech.edu (S. Kumar).

https://doi.org/10.1016/j.carbon.2018.03.078
0008-6223/

determination of chemical reactions between the PAN-co-MAA and CNC during the stabilization process, and the structural differences between the neat materials and the composites. In addition, by providing a more complete understanding of the stabilization of PAN-based films with CNC fillers, this study could give greater insight to the stabilization of both carbon fiber and other carbon materials such as films and bulk material.

2. Experimental

2.1. Materials

Polyacrylonitrile-co-methacrylic acid (PAN-co-MAA; 4 wt% of MAA content, viscosity average molecular weight: 2.47×10^5 g/mol) was obtained from Exlan Co., Japan. Freeze dried CNC (lot# 2012-FPL-CNC-48/051) was produced by USDA Forest Service – Forest Product Laboratory (FPL), and received from the University of Maine, US. Dimethylformamide (DMF) was obtained from Sigma-Aldrich co. and was distilled before use.

2.2. Film and fiber preparation

The procedure used for the preparation of neat PAN-co-MAA, PAN-co-MAA/CNC composites, and neat CNC films followed the process described in the study by Luo et al. [31], except for the neat CNC film the CNC were dispersed in DMF rather than water. The PAN-co-MAA solution and PAN-co-MAA/CNC suspensions were made with a target solid content of 3.7 wt%. The total amount of DMF used for each solution and suspension was 100 mL. For the PAN-co-MAA/CNC suspensions an amount of CNC dependent on the final CNC concentration desired was dispersed in 100 mL of DMF in a bath sonicator (Branson 3510R-MT, 100 W, 42 kHz) for 24 h. The CNC/DMF suspension was then added to PAN-co-MAA powder to reach a total solid content to 3.7 wt%. Then this CNC/PAN-co-MAA/DMF mixture was stirred in a glass reactor at 70 °C and 200 rpm for 3–4 h. For the neat PAN-co-MAA solution the same procedure was followed with the exception of the dispersion of CNC; no dispersion of CNC was required. After stirring the solution/suspensions for 3–4 h, it was poured into a glass jar and degassed in a vacuum oven at 70 °C under vacuum for 5 min. This whole procedure results in a solution/suspension with a solid content around ~4 wt%. Four hours after the solution/suspensions were poured into the glass jar it was cast into a glass mold and dried in an oven with air flow at 70 °C. The neat CNC film was made by dispersing CNC in DMF at 1 wt% for 24 h in a bath sonicator and then cast the same way as the PAN-co-MAA and PAN-co-MAA/CNC composite films. Seven different compositions of films were made with 0, 5, 10, 20, 30, 40, and 100 wt% CNC with respect to the weight of the PAN-co-MAA, and these samples will be referred to as neat PAN-co-MAA, CNC-5, CNC-10, CNC-20, CNC-30, CNC-40, and neat CNC, respectively. All the films had a thickness of ~100 μm. A 13 μm thick PAN-co-MAA film was also made with a similar process to determine the effect of surface area to volume ratio on differential scanning calorimetry (DSC) and thermogravimetric analysis (TGA).

The neat PAN-co-MAA fiber was also made by a previously described process [30]. First 15 g of PAN-co-MAA was dissolved in 100 mL of DMF at 80 °C and stirred at 200 rpm for 3–4 h. The fiber was spun with a spinning unit with a 200 μm diameter spinneret (Hills Inc.). The solution was gel spun by spinning into −50 °C methanol with an air gap of ~5 cm, and the as spun ratio was 3x. Afterwards the fiber was the kept at −50 °C in methanol for 1 day. The fiber was subsequently drawn at room temperature followed by hot drawing in a glycerol bath (165 °C). The final draw ratio of the fiber was 15x with a diameter of ~15 μm.

2.3. Characterization

DSC was ran on TA instrument Q100. Sample sizes of 2–3 mg were used in standard aluminum pans. Samples were heated from 50 to 400 °C at a heating rate of 5, 10, 15, and 20 °C/min in nitrogen and then rerun in air. Samples were also run directly in air at a heating rate of 10 °C/min. Weight change with temperature change was investigated using TGA with an TA instruments Q500. Samples were heated from 50 to 400 °C at a heating rate of 5 °C/min in nitrogen then rerun in air. Fourier transform infrared spectroscopy (FTIR) was performed on a Spectrum One spectrometer (PerkinElmer Inc). The tests were done by grinding films with KBr and pressing a pellet. The scan range was 700–4000 cm^{-1} with resolution of 4 cm^{-1}. Wide-angle X-ray diffraction (WAXD) experiments were completed on a Rigaku MicroMax-002 (CuK_α, $\lambda = 0.1542$ nm) equipped with a Rigaku R-axis IV++ detector. MDI Jade 9 software was used to analyze the WAXD pattern. FTIR and WAXD were performed on neat PAN-co-MAA, neat CNC, and CNC-40 before heating and after heating the samples to different temperature under different environments. Unless specifically mentioned all experiments were done on cast films with ~100 μm thickness.

3. Results and discussion

The stabilization of PAN is typically done between 200 and 300 °C and the reactions contain dehydrogenation, cyclization, oxidation, and crosslinking as shown in Fig. 1 [1]. Cyclization can occur in inert atmosphere, while the oxidation requires the presence of oxygen. Crosslinking can occur to a small degree in an inert atmosphere during stabilization by intermolecular cyclization, but is much more prominent in an oxygen atmosphere after the oxidation reaction. This allows separating the cyclization reaction from the oxidation reaction by first running the sample in an inert atmosphere, such as nitrogen, then followed by air [2,10]. The proposed reaction for the stabilization of cellulose by Tang and Bacon (Fig. 2) contains dehydration (150–240 °C), thermal cleavage of the bridge oxygen and the pyranose ring also referred to as depolymerization (240–400 °C), and is followed by aromatization (400–700 °C) [14,16,18,32,33].

3.1. Effect of sample geometry on stabilization

To determine if geometry had an effect on the stabilization reaction, neat PAN-co-MAA fibers (15 μm diameter) and films (13 μm or ~100 μm thick) were tested in DSC. Initial heating runs in nitrogen showed that the magnitude of the cyclization peak between the fiber and films were similar (Fig. 3a). In contrast, when the samples were rerun in air after nitrogen, there was a significant difference on the magnitude of the exothermic reaction that was based on sample geometry (Fig. 3b). The fibers had an exothermic reaction about 4 times the magnitude of the 93 μm thick films and 2 times the magnitude of the 13 μm thick films. This effect of sample geometry on the reaction is believed to result from the rate of oxygen diffusion through the sample, which is dependent on the surface to volume ratio (SA:V). The PAN-co-MAA fibers have about 12 times the SA:V of the 93 μm film, and about 1.7 times the SA:V of the 13 μm film based on the geometry (see supporting information for calculations). The low magnitude of the exothermic reactions for the ~100 μm thick films made it difficult to determine the peak

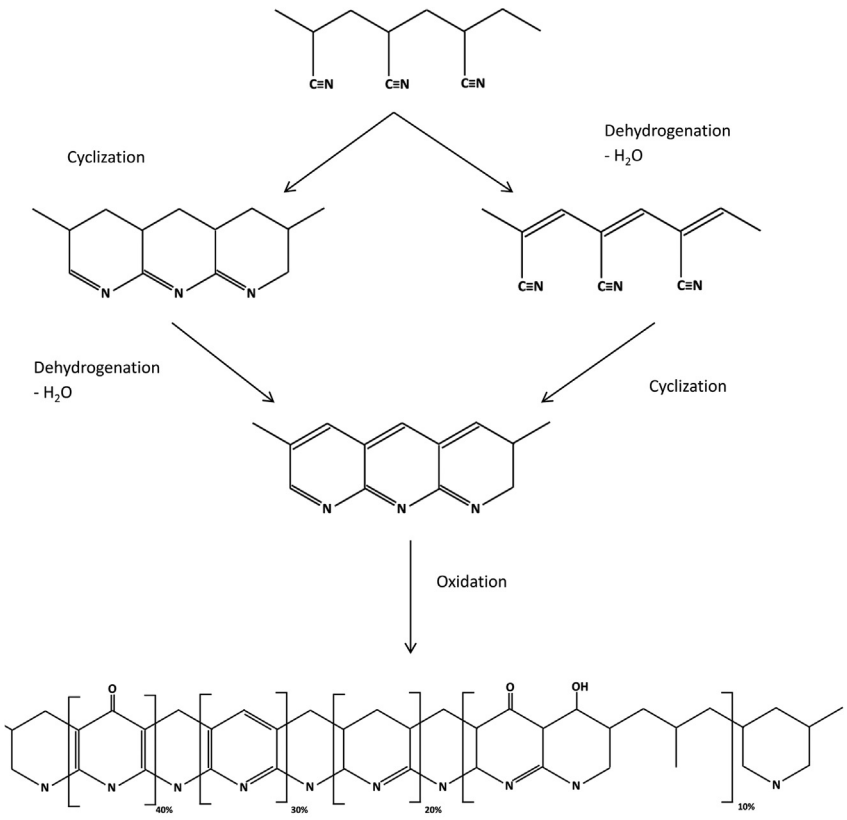

Fig. 1. Proposed chemical pathway for PAN stabilization [13,34].

temperature of crosslinking, which can typically be determined on fibers [2,3]. Note that the ~100 μm thick films were used for the rest of the study, and thus the crosslinking temperatures were not determined. The effect of sample geometry can also be seen in the TGA curves (Fig. 4). It was previously reported that weight gain can be observed in neat PAN fiber due to oxidation if the sample was first run in nitrogen followed by air [2]. In the current study, this was also observed, where for the PAN-co-MAA fiber TGA run in air after nitrogen there was an increase in weight of the neat PAN-co-MAA. The effect of sample geometry on weight gain was present, in which the fiber reached a max of 105% weight percent, the13 μm thick film reached a max of 101% weight percent, while the 93 μm thick film did not experience an increase in weight throughout the run. Even though the 93 μm thick film shows no apparent weight gain, oxidation to some degree likely occurred, though at a lower extent compared to the samples with higher specific surface area, and it is considered here that the mass gained by oxygen pick-up was offset by mass loss due to other reactions.

3.2. Effect of CNC additions on oxygen permeability

It has been hypothesized that the low permeability of oxygen for PAN ($3*10^{-4}$ to $6*10^{-3}$ barrer) is a contributing factor to a skin-core morphology that exists in stabilized and carbonized fiber [35–38]. If the oxygen permeability of CNC or the CNC/PAN interface is higher than PAN, then the addition of CNCs could help provide a fast pathway for oxygen to travel within PAN, particularly if there is a percolated CNC network. This would lead to a more homogenous stabilization of the PAN, and could help prevent the skin-core morphology from forming, and possibly reduce the stabilization time. The range of reported permeability of CNC films is between $6.3*10^{-4}$ to 140.7 barrer [39,40]. Partial support for CNC having higher oxygen permeability than PAN-co-MAA was found in the current study, where weight gain was observed in air rerun for the CNC film, but not the PAN-co-MAA and CNC-40 films (Fig. 5). The diffusion of oxygen through the PAN-co-MAA on the surface in the CNC-40 sample is likely limiting the oxygen to the sample, which is why we do not see weight gain. Though we do not see weight gain, a more homogenous stabilization should still occur in the composite samples because of the CNC network for oxygen diffusion into the film.

3.3. Effect of CNC additions on PAN cyclization

The results of the DSC measurement in nitrogen for neat PAN-co-MAA, neat CNC, and PAN-co-MAA/CNC composite films are summarized in Table 1, while Fig. 6 shows DSC plots of the sample ran in different environments at a heating rate of 10 °C/min. As reported in the literature at this heating rate the cyclization reaction of PAN has an exothermic peak around ~275 °C, which is similar to what was measured for the PAN-co-MAA used in this study for the various heating rates. In contrast, CNC have an

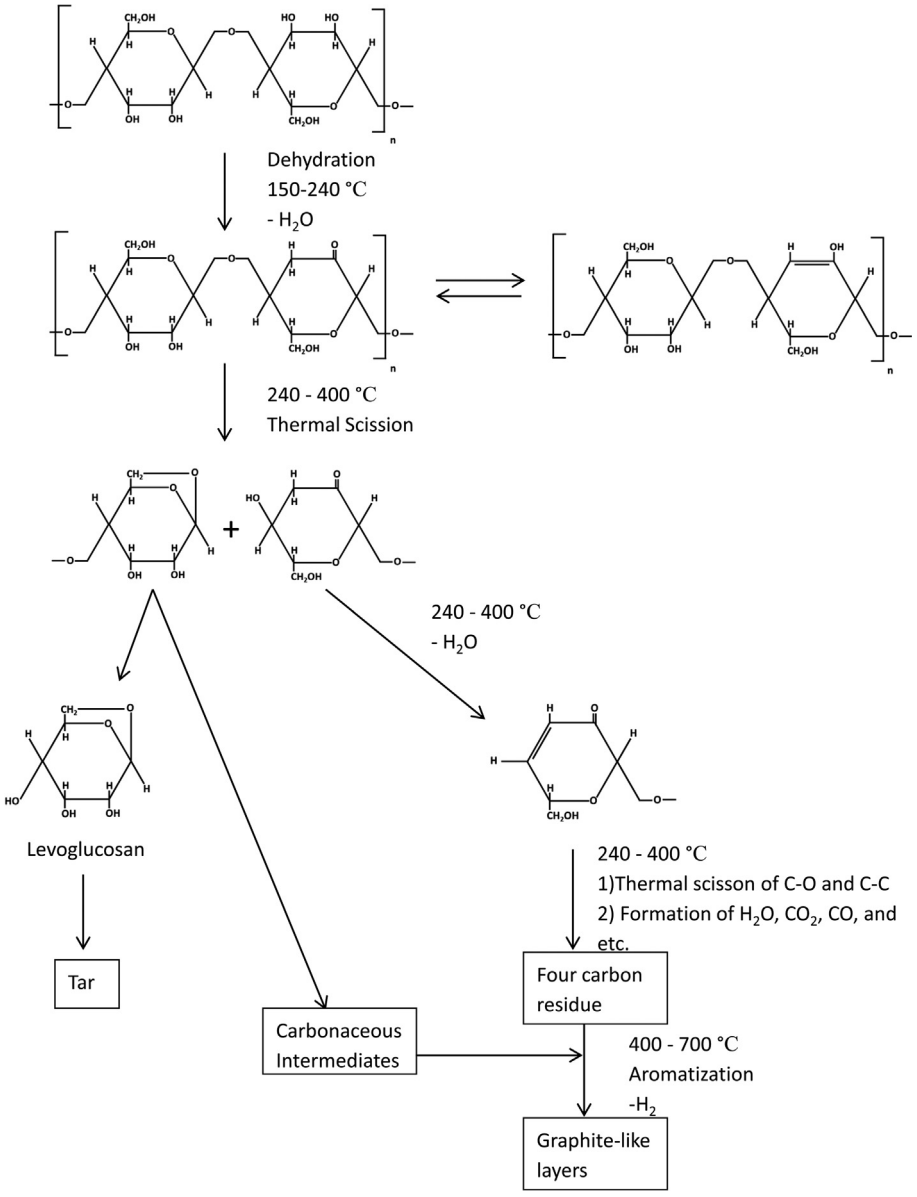

Fig. 2. Proposed chemical pathway for cellulose stabilization and carbonization [16].

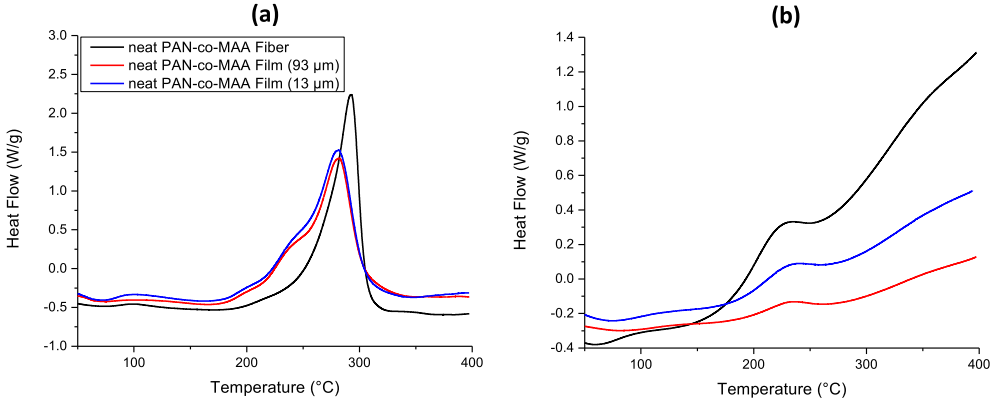

Fig. 3. DSC curves comparing neat PAN-co-MAA fiber vs film at a heating rate of 10 °C/min. **(a)** in nitrogen **(b)** in air after being run in nitrogen. (A colour version of this figure can be viewed online.)

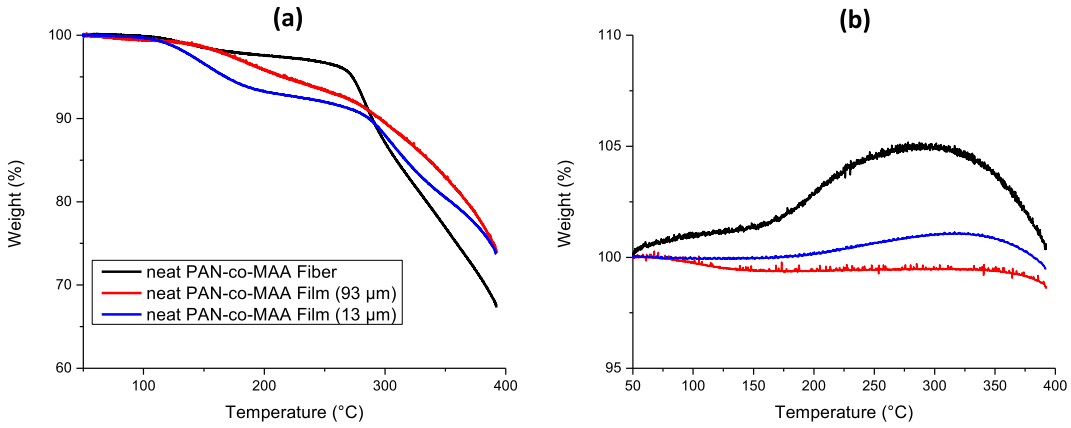

Fig. 4. TGA curves at a heating rate of 5 °C/min to show differences showing differences between film and fibers, and influence of thickness on films. **(a)** in nitrogen **(b)** in air after run in nitrogen. (A colour version of this figure can be viewed online.)

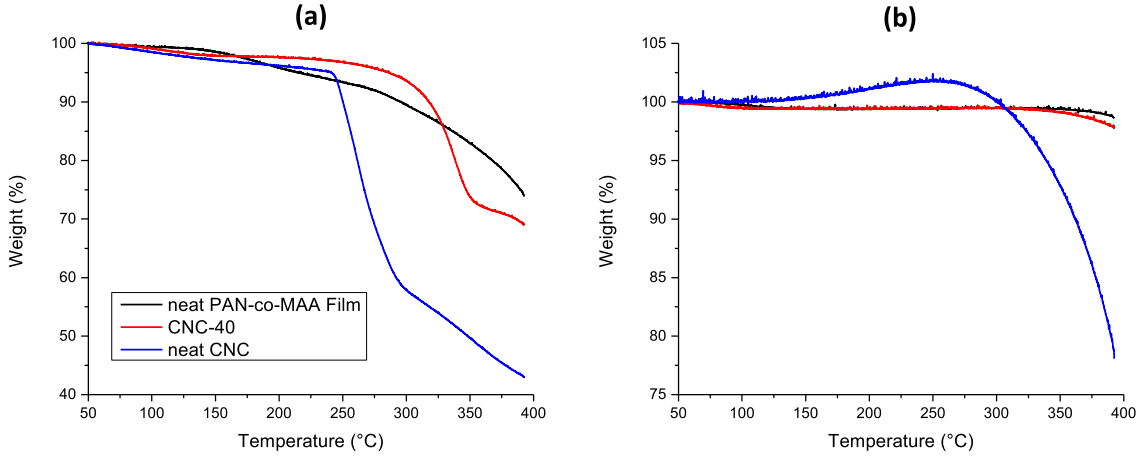

Fig. 5. TGA curves of films at a heating rate of 5 °C/min to show differences neat PAN-co-MAA, neat CNC, and CNC-40. **(a)** in nitrogen **(b)** in air after run in nitrogen. (A colour version of this figure can be viewed online.)

Table 1
Summary of the onset and peak temperatures in the film DSC runs in nitrogen.

Sample	neat PAN-co-MAA	CNC-5	CNC-10	CNC-20	CNC-30	CNC-40	neat CNC
Onset of cyclization temperature @ 5 °C/min (°C)	196	199	200	204	207	218	N/A
Onset of cyclization temperature @ 10 °C/min (°C)	208	212	211	217	221	228	N/A
Onset of cyclization temperature @ 15 °C/min (°C)	213	218	219	224	229	237	N/A
Onset of cyclization temperature @ 20 °C/min (°C)	222	224	224	229	235	242	N/A
Cyclization peak temperature @ 5 °C/min (°C)	265	262	262	267	268	270	N/A
Cyclization peak temperature @ 10 °C/min (°C)	275	271	274	278	278	282	N/A
Cyclization peak temperature @ 15 °C/min (°C)	280	279	280	284	285	288	N/A
Cyclization peak temperature @ 20 °C/min (°C)	284	284	285	289	290	293	N/A
2nd exothermic peak temperature @ 5 °C/min (°C)	N/A	N/A	N/A	356	352	349	361
2nd exothermic peak temperature @ 10 °C/min (°C)	N/A	N/A	N/A	370	364	361	372
2nd exothermic peak temperature @ 15 °C/min (°C)	N/A	N/A	N/A	378	373	370	380
2nd exothermic peak temperature @ 20 °C/min (°C)	N/A	N/A	N/A	386	380	375	387

endothermic peak ~275 °C that is related to dehydration and thermal scission of the of bridge oxygen [16,41]. For cellulose, it has been reported that smaller particles and more compressed samples (e.g., more contact between cellulose) leads to lower thermal stability, [42,43]. In the current study, neat CNC materials tested in DSC (heating rate of 10 °C/min) had a different curve shape, enthalpy of the endothermic reaction, and over 35 °C difference for the onset of dehydration, depending on how the CNC was prepared (e.g., solvent used to cast film, if the film was ground to a powder, or as received freeze dried CNC powder) (Fig. S1 and Table S1). The CNC

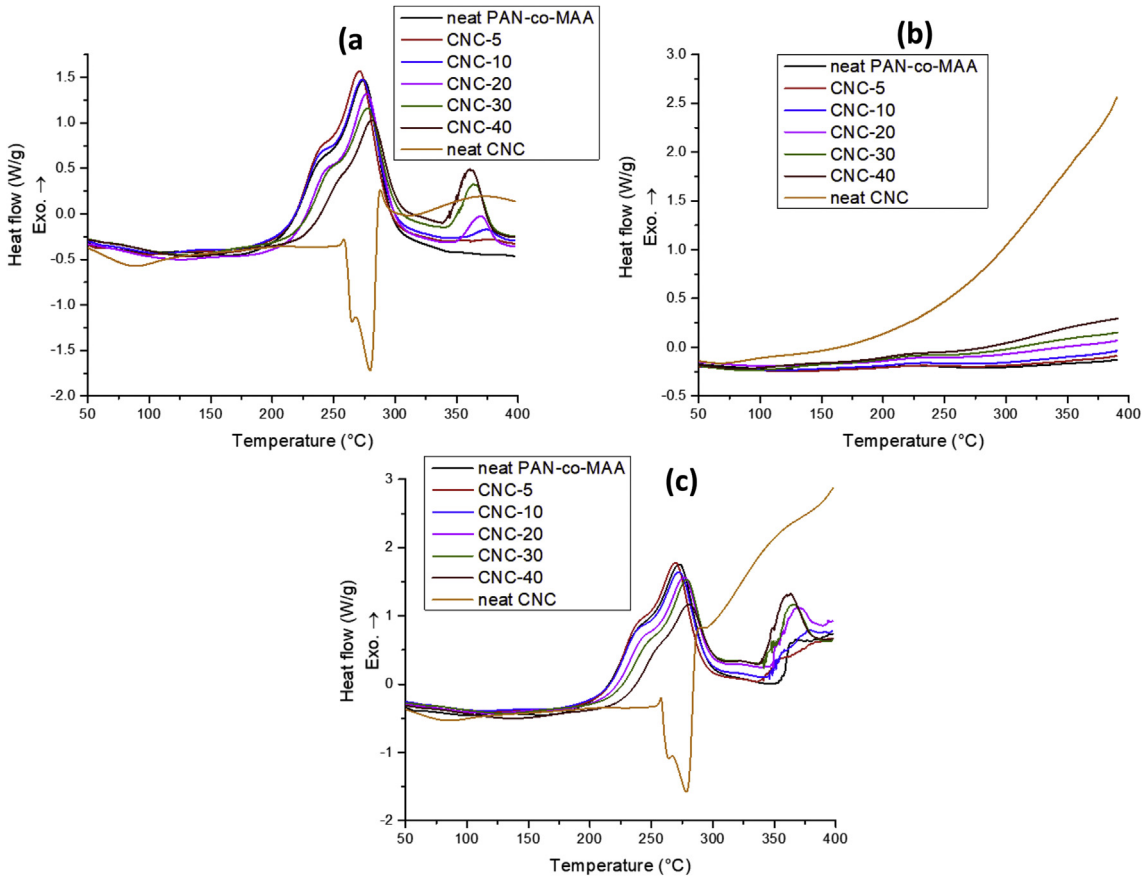

Fig. 6. DSC runs of the film samples at a heating rate of 10 °C/min in **(a)** nitrogen, **(b)** rerun in air after nitrogen, and **(c)** directly in air. (A colour version of this figure can be viewed online.)

samples with higher surface area (e.g., ground films and freeze dried CNC powders) had higher thermal stability and enthalpy of reaction. Freeze dried CNC was the most thermally stable and was heavily aggregated at the microscale as seen in previous studies [30,42]. For the PAN-co-MAA/CNC composite films, the dispersion of CNC was fairly good in that no micron sized agglomeration were observed [31], which should result in higher thermal stability of the CNC. For consistency in the measurements, in the rest of the paper only as casted film samples were tested.

In general the cyclization peak temperatures increased with increasing CNC loading at all heating rates (Table 1). However, for the CNC-5 and CNC-10 films there was either no change or a decrease in peak temperature compared to the neat PAN-co-MAA at heating rates of 15 °C/min and lower. It has been previously reported by Liu et al. [2] that the addition of 1 wt% CNT into PAN also exhibited an increase in cyclization peak temperature. Additionally, Mathur et al. [44] reported that the DSC run of PAN fibers in air exhibited a higher onset and peak temperature for cyclization than when the sample was run in nitrogen. The presence of oxygen in CNC may be a contributing factor to the increased higher onset and peak temperature for cyclization. The shape of the cyclization curves were very similar between neat PAN-co-MAA and the PAN-co-MAA/CNC composites with minimal changes with increasing CNC loading. The lack of change in curve shape indicates that the dehydration reaction of the CNC may not have occurred during PAN cyclization, which is supported by FTIR and WAXD.

3.4. Increased thermal stability of cellulose nanocrystals in polyacrylonitrile

Both FTIR and WAXD results indicate that chemical and structural breakdown of the CNC was shifted to higher temperatures for the PAN-co-MAA/CNC composites as compared to neat CNC. For neat CNC films the FTIR spectra (Fig. 7b) show that after heating the CNC film to 310 °C, peaks associated with cellulose at 1161 (COC in pyranose ring), 1113 (ring stretch), 1061 (CO or COH on ring or bridge oxygen stretch), and 1033 cm^{-1} (CO) started to lose their sharpness and started to merge [45,46]. Likewise, WAXD patterns (Fig. 8) show the disappearance of the peaks associated with cellulose II ($2\theta = 20.4°$) and cellulose I ($2\theta = 22.6°$), indicating structural breakdown of the cellulose [42,47–49]. In contrast, for the CNC-40 composite heated to 310 °C, the FTIR spectra maintain distinct peaks at 1161, 1113, 1061, and 1033 cm^{-1}, and the WAXD retain the peaks associated with cellulose I and II, supporting the conclusion that dehydration and depolymerization of CNC had not occurred. It is considered here that having a fine CNC dispersion

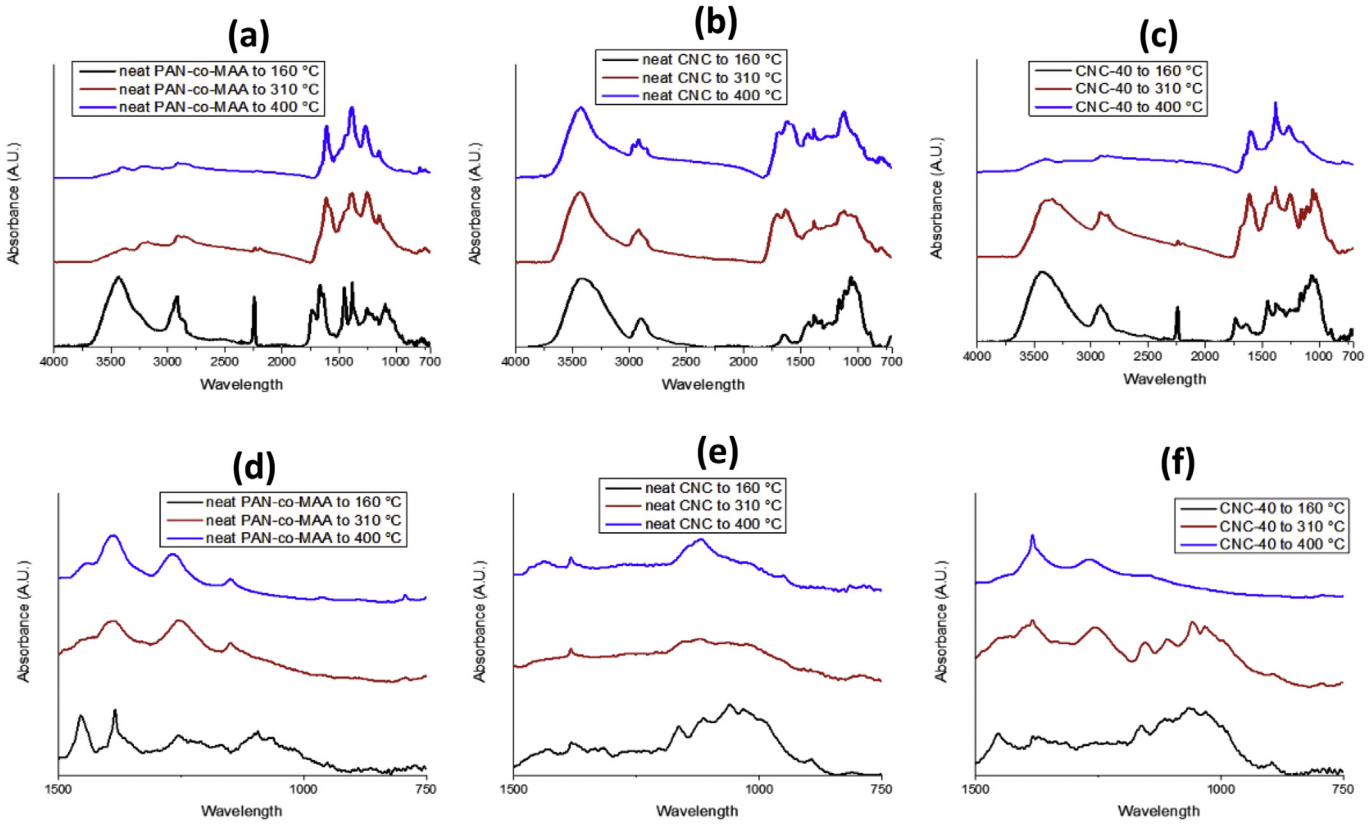

Fig. 7. FTIR plots of **(a)** neat PAN-co-MAA, **(b)** neat CNC, and **(c)** CNC-40 from 4000 to 650 cm^{-1}, and **(d)** neat PAN-co-MAA, **(e)** neat CNC, and **(f)** CNC-40 from 1500 to 750 cm^{-1} after being heated at 10 °C/min in nitrogen. (A colour version of this figure can be viewed online.)

within PAN-co-MAA, which was previously seen [31], could be one mechanism in retarding the dehydration and depolymerization reactions to CNCs.

3.5. Effect of CNC additions on cyclization activation energy and reaction rates

The average enthalpy of reaction during cyclization over the four heating rates can be found in Table 2. The composite samples' enthalpy of cyclization is similar to the weight fraction of PAN-co-MAA it is composed of, though the values calculated by PAN-co-MAA weight fraction are still slightly higher than the experimental values. This discrepancy between the calculated and experimental value is likely due to heat released during cyclization is being absorbed by the CNC in the composite. Using the cyclization peak temperature at different heating rates, the activation energy of cyclization (Fig. 9a and Table 3) can be calculated with Kissinger's equation (equation (1)) [50] where E_a, R, ϕ, and T_p are activation energy (kJ/mol), universal gas constant (8.314 J/(mol*K)), heating rate (K/min), and reaction peak temperature (K), respectively. It was found that the activation energy decreased in all composite samples to a consistent value of ~147 kJ/mol (~16% decrease) compared to the from neat PAN-co-MAA sample value of 175 kJ/mol. Using the activation energy the reaction rate constant (k) can be calculated with equation (2), while the pre-exponential factor, A, can be determined from equation (3), where T is the temperature (K) at which the reaction rate is being solved [3,51]. The temperature has large effect on the reaction rate constant, so the reaction rate constant was solved for a heating rate of 10 °C/min at 200, 250, and 300 °C. These temperatures were chosen because PAN is often stabilized between 200 and 300 °C [12,33,34].

$$-\frac{\mathbf{E_a}}{\mathbf{R}} = \frac{\mathbf{d}\left(\ln\frac{\phi}{\mathbf{T_p^2}}\right)}{\mathbf{d}\left(\frac{1}{\mathbf{T_p}}\right)} \quad (1)$$

$$\mathbf{k} = \mathbf{A}e^{-\mathbf{E_a}/\mathbf{RT}} \quad (2)$$

$$\mathbf{A} = \frac{\phi \mathbf{E_a} e^{\mathbf{E_a}/\mathbf{RT_p}}}{\mathbf{RT_p^2}} \quad (3)$$

As summarized in Table 3, the cyclization reaction rate constant for both the neat PAN-co-MAA and the composites increases with increasing T. For the composites, increasing CNC loading results in a lower reaction rate constant, the extent of which was dependent on T. Interestingly, the effect of CNC additions to on the cyclization reaction rate constant of the neat PAN-co-MAA was dependent on T. For example, at 200 °C all composite samples had a higher reaction rate constant than neat PAN-co-MAA, while at 300 °C the opposite was true with neat PAN-co-MAA having the highest reaction rate constant.

3.6. Development of a 2nd exothermic peak in composite samples

A 2nd exothermic peak in DSC developed in the PAN-co-MAA/CNC composite samples above 300 °C in nitrogen (Fig. 6), which did not occur in the neat PAN-co-MAA samples. The activation energy of this 2nd exothermic peak (Fig. 9b and Table 3) was calculated for CNC-20 and higher CNC loaded samples. At the lower CNC loadings the curves were not perfectly smooth making it difficult to determine the peak temperature. There was a trend of

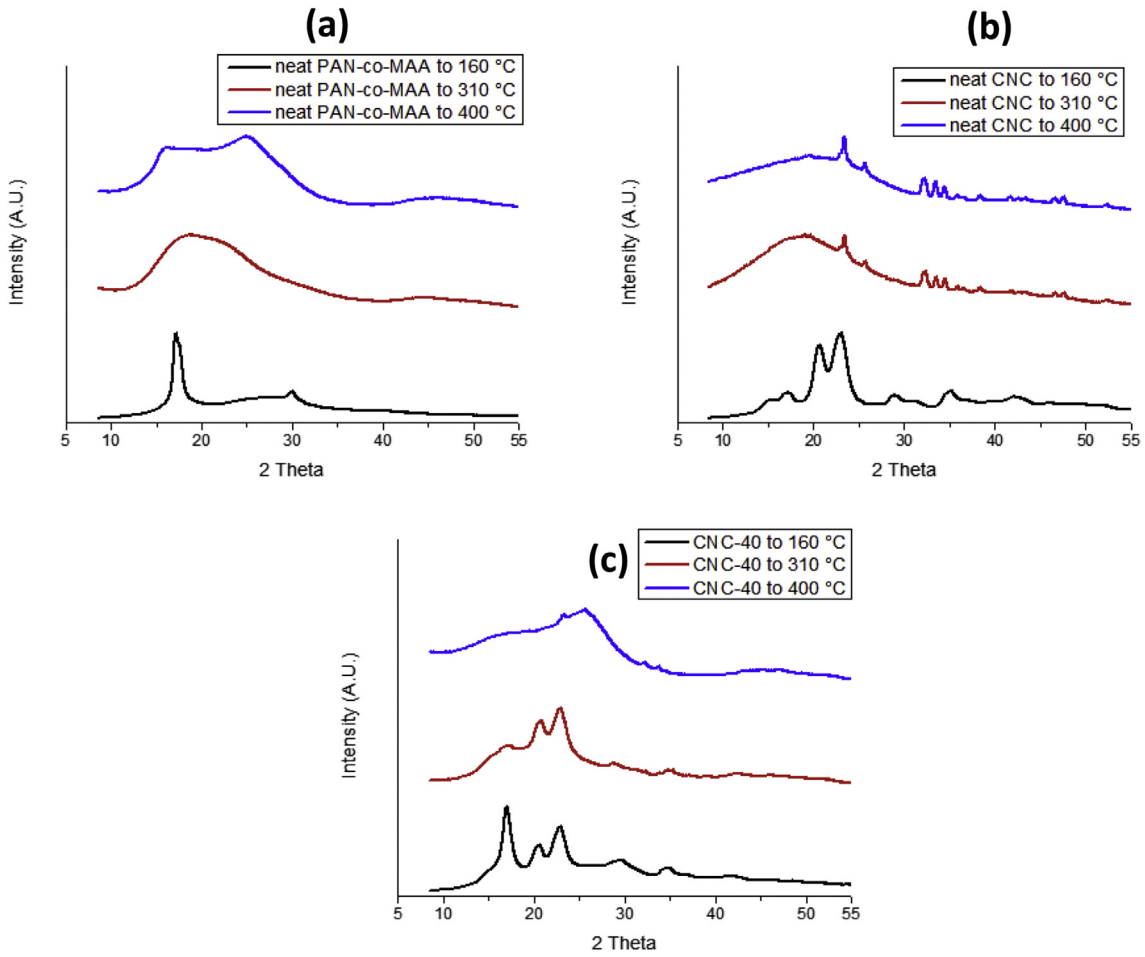

Fig. 8. WAXD plots of **(a)** neat PAN-co-MAA, **(b)** neat CNC, and **(c)** CNC-40 after being heated at 10 °C/min in nitrogen. (A colour version of this figure can be viewed online.)

Table 2
Experimentally measured and the rule of mixtures estimate of enthalpy of cyclization, which shows similar values indicating CNC is not reacting at this temperature.

Sample	neat PAN-co-MAA	CNC-5	CNC-10	CNC-20	CNC-30	CNC-40
Experimental average enthalpy of cyclization (J/g)[a]	648	607	569	494	412	344
Theoretical enthalpy of cyclization as function of PAN-co-MAA weight percent (J/g)	648	615	583	518	453	389

[a] Average of the runs ran at a heating rate of 5, 10, 15, and 20 °C/min.

increasing activation energy with increasing CNC loading, with the neat CNC sample having the highest activation energy of 174 kJ/mol.

The formation of this 2nd exothermic peak is considered to result from; i) CNC reactions interactions, ii) PAN-co-MAA/CNC interactions, or iii) a combination of these two reactions occurring simultaneously. This exothermic reaction in neat CNC is associated with a mixture of dehydration, decarbonylation, decarboxylation, and the formation of levoglucosan, which forms gaseuous products like CO, CO_2, CH_4, and H_2O [16,52]. For the composite samples the exothermic peak was sharper than in the neat CNC sample, and shifts to lower temperatures with increasing CNC loading, where at 40 wt% CNC loading the shift was ~10 °C lower than for the neat CNC. Since there were no dehydration or depolymerization reactions observed at lower temperatures, it is possible that there is either a change in the reaction kinetics of cellulose or a different set of reactions are occurring in the cellulose.

The 2nd exothermic peak could also be due to reactions between PAN-co-MAA and CNC, four proposed reactions are given in Fig. 10. The proposed reactions are based on the degradation pathway of cellulose and the oxidation pathways of PAN, because according to our experiments cellulose has not undergone depolymerization and PAN has not undergone oxidation before this exothermic peak. In support of reactions between PAN-co-MAA and CNC, the TGA data (Fig. 5 and Table 4) shows that the experimental yield of CNC-40 is higher than the rule of mixture yield of the PAN-co-MAA and CNC after heating to 400 °C. One of the ways CNC could interact with PAN-co-MAA is by supplying oxygen needed for reactions. As a result of depolymerization of CNC, oxygen could be made available that would promote a reaction with PAN-co-MAA. In partial support for this, DSC results of the neat PAN-co-MAA ran directly in air (Fig. 6) show an exothermic reaction that occurs after cyclization while in nitrogen this does not occur.

3.7. Effect of CNC additions on oxidation activation energy and reaction rates

DSC of films ran in nitrogen and then re-ran in air (Fig. 6) show a

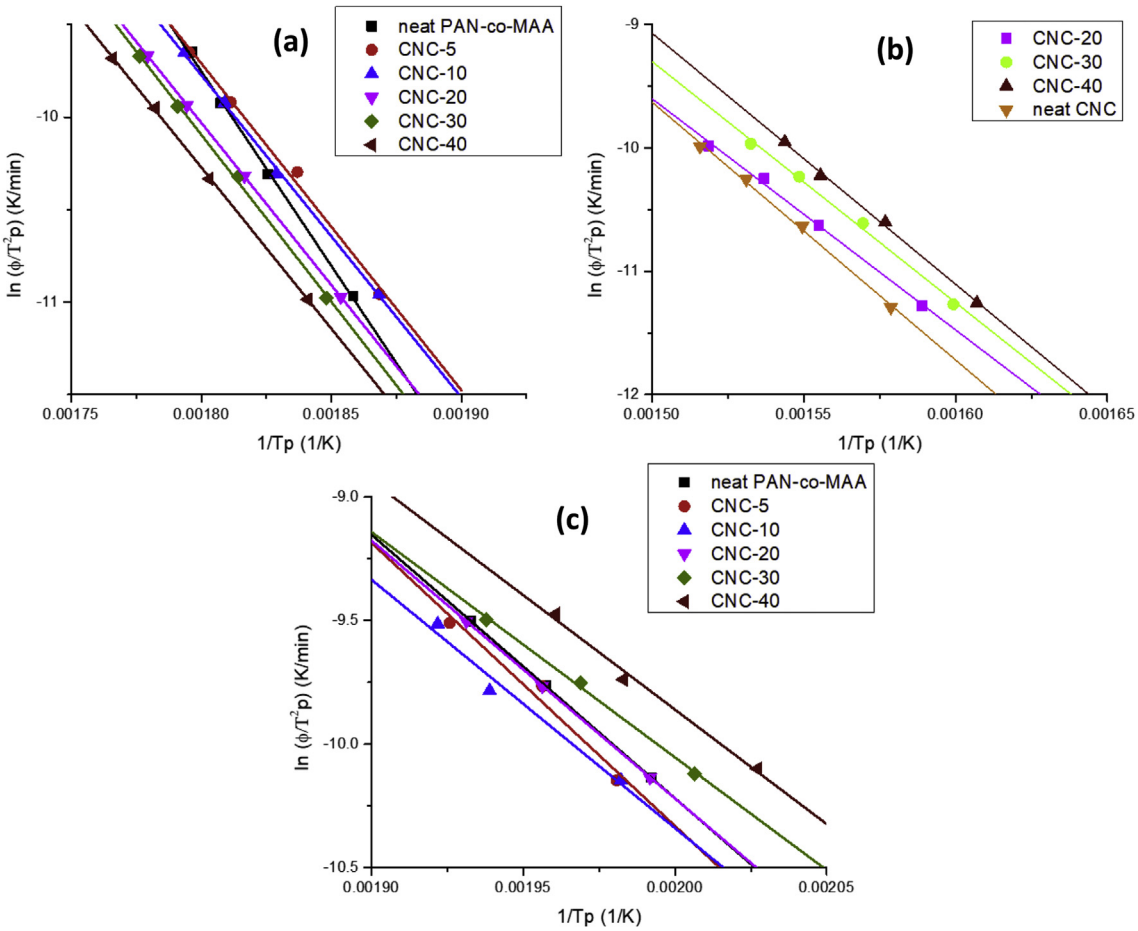

Fig. 9. Graphs used to calculate the activation energy of the **(a)** cyclization of film samples in nitrogen atmosphere, **(b)** 2nd exothermic reaction in the film samples in nitrogen atmosphere, and **(c)** oxidation of film samples re-run in air after being run initially in nitrogen. (A colour version of this figure can be viewed online.)

Table 3
Activation energy, pre-exponential factor (A), and reaction rate constant (k) for cyclization, 2nd exothermic peak, and oxidation, calculated from DSC measurements at different heating rates using Kissinger's method. The results of the cyclization and 2nd exothermic peak were from experiments conducted in nitrogen, while the oxidation results were done in air after first running the sample in nitrogen.

Sample	neat PAN-co-MAA	CNC-5	CNC-10	CNC-20	CNC-30	CNC-40	neat CNC
Activation Energy of Cyclization (kJ/mol)	175	147	145	146	150	145	N/A
A for cyclization (s^{-1})	3.3×10^{16}	7.4×10^{13}	4.0×10^{13}	4.0×10^{13}	1.0×10^{14}	2.5×10^{13}	N/A
k of cyclization @ 200 °C (s^{-1})	0.0016	0.0044	0.0040	0.0031	0.0026	0.0025	N/A
k of cyclization @ 250 °C (s^{-1})	0.11	0.17	0.14	0.11	0.10	0.09	N/A
k of cyclization @ 300 °C (s^{-1})	3.8	3.0	2.5	2.0	2.1	1.6	N/A
Activation Energy of 2nd exothermic peak (kJ/mol)	N/A	N/A	N/A	156	162	169	174
Activation Energy of Oxidation (kJ/mol)	89	95	84	87	76	77	N/A
A for oxidation (s^{-1})	7.0×10^{8}	3.2×10^{9}	1.8×10^{8}	4.4×10^{8}	3.3×10^{7}	5.4×10^{7}	N/A
k of oxidation @ 200 °C (s^{-1})	0.12	0.10	0.11	0.12	0.14	0.17	N/A
k of oxidation @ 250 °C (s^{-1})	0.99	0.99	0.80	0.95	0.87	1.10	N/A
k of oxidation @ 300 °C (s^{-1})	5.87	6.67	4.27	5.42	3.98	5.18	N/A

larger exothermic reaction for neat CNC films than for neat PAN-co-MAA films. The CNC reaction with oxygen could be more exothermic than PAN or it is possible that the pure CNC films used in the study had a higher surface area due to surface roughness and/or porosity. It has previously been reported that casted CNC films are typically not fully dense [53]. This leads to an increase in the oxygen diffusion rate thus leading to the much higher exothermic reaction. Similarly to when PAN fibers are rerun in air the exothermic reaction was much higher than the PAN films, presumably due to the large surface area to volume ratio in the fibers leading to higher oxygen diffusion rates (Fig. 3). The DSC curves of the composite films do not follow the rule of mixture, being much less exothermic than expected. This could be a result of the composite films having much less porosity than the pure CNC films, or that PAN-co-MAA having lower oxygen permeability than CNC, making the oxygen diffusing through the PAN-co-MAA the

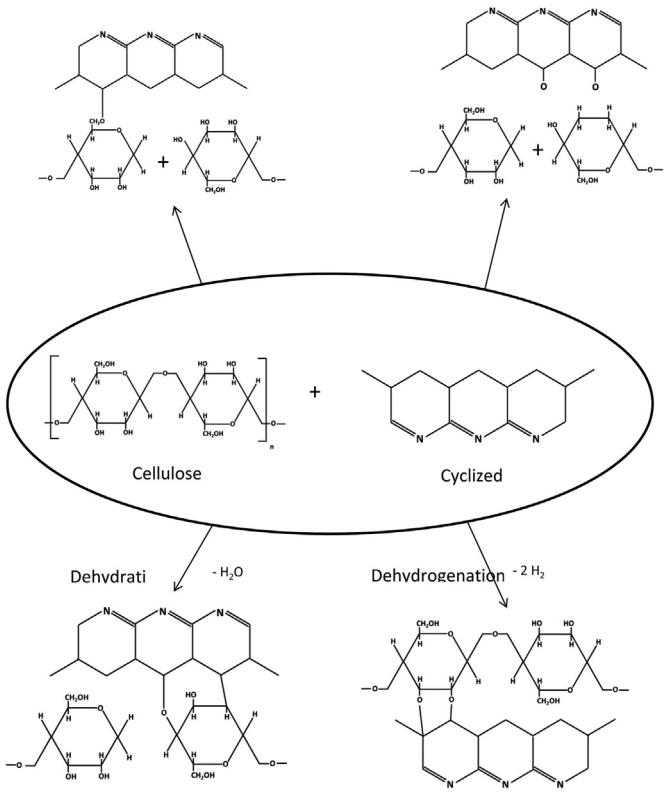

Fig. 10. Proposed possible chemical reactions between PAN and cellulose during stabilization.

limiting factor for the CNC reaction. The FTIR and WAXD of the samples can be found in Figs. S2 and S3.

The activation energy of oxidation (Fig. 9c and Table 3) was calculated with Kissinger's equation (equation (1)), using the oxidation peak temperature at different heating rates (Table 5). At low CNC loadings (5 and 10 wt%) the oxidation peak temperature increases compared to neat PAN-co-MAA, while at higher CNC loadings the peak temperature decreases. It is considered here that oxygen in the CNC facilitates the oxidation of PAN, which is more energetically inclined during the first nitrogen run. The decrease in peak temperature at higher CNC loadings is considered to result from a larger presence of oxygen and potentially faster diffusion path along a percolated CNC network within the PAN-co-MAA. Interestingly, Liu et al. [2] reported that at low CNT loadings (1 wt %) the oxidation peak temperature also increased.

As summarized in Table 3, there was a small effect of CNC additions to PAN-co-MAA on the activation energy of oxidation and on the oxidation reaction rate constants. With increased CNC loadings within the composite samples, there was a weak trend of decreasing activation energy, but the oxidation reaction rate constant showed no consistent trends (at all temperatures). With increasing T, the oxidation reaction rate constant for both the neat PAN-co-MAA and the composites decreases. At certain CNC loadings and temperatures, the oxidation reaction rate constant was higher than neat PAN-co-MAA. Interestingly, at 200 °C samples CNC-20, CNC-30, and CNC-40 had higher (or the same) reaction rate constant for both cyclization and oxidation than neat PAN-co-MAA. This indicates conditions in which the addition of CNC into PAN-co-MAA can reduce the energy needed for stabilization.

4. Conclusion

With the addition of CNC to PAN-co-MAA there was a 16% reduction in the activation energy of the PAN cyclization reaction, the extent of which did not change with CNC loading. In contrast, the activation energy of oxidation was minimally affected by CNC additions. At certain CNC loadings and temperatures, the reaction rate constant for both cyclization and oxidation where higher for PAN-co-MAA/CNC composites than for neat PAN-co-MAA, indicating that the addition of CNC into PAN-co-MAA can reduce the energy needed for stabilization. The PAN-co-MAA onset of cyclization temperature increased with CNC loadings. The peak temperature of cyclization, as compared to the neat PAN-co-MAA, was shifted to lower temperatures at low CNC loadings and low heating rates, while at higher CNC loadings and higher heating rates it was shifted to higher temperatures. Additionally, CNC within the PAN-co-MAA/CNC composite were more stable than the neat CNC films. DSC showed that the PAN-co-MAA/CNC composites did not exhibit the dehydration reaction seen in neat CNC films that occurs at ~275 °C, while FTIR and WAXD showed that the chemical and structural changes in CNC occurred at higher temperatures. Lastly, the oxidation reaction of PAN-co-MAA was influenced by the surface area to volume ratio of the sample that was tested, (e.g., fiber, 13 μm thick film, 93 μm thick film), while the cyclization reaction was unaffected.

Table 4
Yield of the films after running the samples in the TGA at 5 °C/min to 400 °C.

Sample	neat PAN-co-MAA	CNC-40	neat CNC
Experimental yield after run in Nitrogen (wt%)	74	69	43
Experimental yield after rerun in Air (wt%)	99	98	78
Rule of Mixture yield after run in Nitrogen (wt%)	N/A	62	N/A
Rule of Mixture yield after rerun in Air (wt%)	N/A	91	N/A

Table 5
Peak temperature of the oxidation reaction measured via DSC of films run in nitrogen and then re-run in air.

Sample	neat PAN-co-MAA	CNC-5	CNC-10	CNC-20	CNC-30	CNC-40
Oxidation peak temperature @ 10 °C/min (°C)	229	232	232	229	225	220
Oxidation peak temperature @ 15 °C/min (°C)	238	238	243	238	235	231
Oxidation peak temperature @ 20 °C/min (°C)	244	246	247	245	243	237

Acknowledgements

This work was financially supported by the Renewable Bioproducts Institute at Georgia Institute of Technology, the Air Force Office of Scientific Research (Grant# FA9550-14-1-0194), and by the Forest Products Laboratory (USDA grant # 15-JV-11111129-063).

Appendix A. Supplementary data

Supplementary data related to this article can be found at https://doi.org/10.1016/j.carbon.2018.03.078.

References

[1] Y. Liu, H.G. Chae, S. Kumar, Gel-spun carbon nanotubes/polyacrylonitrile composite fibers. Part I: effect of carbon nanotubes on stabilization, Carbon 49 (13) (2011) 4466–4476.
[2] Y. Liu, H.G. Chae, S. Kumar, Gel-spun carbon nanotubes/polyacrylonitrile composite fibers. Part II: stabilization reaction kinetics and effect of gas environment, Carbon 49 (13) (2011) 4477–4486.
[3] H.C. Liu, A.-T. Chien, B.A. Newcomb, A.A.B. Davijani, S. Kumar, Stabilization kinetics of gel spun polyacrylonitrile/lignin blend fiber, Carbon 101 (2016) 382–389.
[4] S. Dalton, F. Heatley, P.M. Budd, Thermal stabilization of polyacrylonitrile fibres, Polymer 40 (20) (1999) 5531–5543.
[5] T.H. Ko, H.Y. Ting, C.H. Lin, Thermal stabilization of polyacrylonitrile fibers, J. Appl. Polym. Sci. 35 (3) (1988) 631–640.
[6] R. Houtz, "Orlon" acrylic fiber: chemistry and properties, Textil. Res. J. 20 (11) (1950) 786–801.
[7] N. Grassie, J. Hay, Thermal coloration and insolubilization in polyacrylonitrile, J. Polym. Sci. Polym. Chem. 56 (163) (1962) 189–202.
[8] A. Standage, R. Matkowsky, Thermal oxidation of polyacrylonitrile, Eur. Polym. J. 7 (7) (1971) 775–783.
[9] G. Henrici-Olive, S. Olive, Inter-versus intramolecular oligomerization of nitrile groups in polyacrylonitrile, Polym. Bull. 5 (8) (1981) 457–461.
[10] Q. Ouyang, L. Cheng, H. Wang, K. Li, Mechanism and kinetics of the stabilization reactions of itaconic acid-modified polyacrylonitrile, Polym. Degrad. Stabil. 93 (8) (2008) 1415–1421.
[11] T.C. Chung, Y. Schlesinger, S. Etemad, A. Macdiarmid, A. Heeger, Optical studies of pyrolyzed polyacrylonitrile, J. Polym. Sci. Polym. Phys. Ed 22 (7) (1984) 1239–1246.
[12] B.A. Newcomb, Processing, structure, and properties of carbon fibers, Compos. Part A: Appl. Sci. Manuf. 91 (2016) 262–282.
[13] H. Chang, J. Luo, P.V. Gulgunje, S. Kumar, Structural and functional fibers, Annu. Rev. Mater. Res. 47 (2017) 331–359.
[14] A.G. Dumanlı, A.H. Windle, Carbon fibres from cellulosic precursors: a review, J. Mater. Sci. 47 (10) (2012) 4236–4250.
[15] M. Sevilla, A.B. Fuertes, The production of carbon materials by hydrothermal carbonization of cellulose, Carbon 47 (9) (2009) 2281–2289.
[16] M.M. Tang, R. Bacon, Carbonization of cellulose fibers—I. Low temperature pyrolysis, Carbon 2 (3) (1964), 211IN1215-214220.
[17] R. Bacon, M. Tang, Carbonization of cellulose fibers—II. Physical property study, Carbon 2 (3) (1964) 221IN3223–222IN4225.
[18] P. Morgan, Carbon Fibers and Their Composites. Materials Engineering, CRC press, Boca Raton, 2005.
[19] H.C. Liu, A.-T. Chien, B.A. Newcomb, Y. Liu, S. Kumar, Processing, structure, and properties of lignin-and CNT-incorporated polyacrylonitrile-based carbon fibers, ACS Sustain. Chem. Eng. 3 (9) (2015) 1943–1954.
[20] D.A. Baker, T.G. Rials, Recent advances in low-cost carbon fiber manufacture from lignin, J. Appl. Polym. Sci. 130 (2) (2013) 713–728.
[21] J.-W. Yang, D.Y. Jin, J.E. Lee, S.G. Lee, W.H. Park, Manufacturing and characteristics of PAN-based composite carbon fibers containing cellulose particles, Carbon Lett. 16 (3) (2015) 203–210.
[22] M.I. Kim, M.-S. Park, Y.-S. Lee, Cellulose-based carbon fibers prepared using electron-beam stabilization, Carbon letters 18 (1) (2016) 56–61.
[23] T.A. Edison, Manufacture of Filaments for Incandescent Electric Lamps, US470925 A, 1892.
[24] S.-J. Park, in: R. Hull, C. Jagadish, Y. Kawazoe, R.M. Osgood, J. Parisi, T.-Y. Seong, S.-i. Uchida, Z.M. Wang (Eds.), Carbon Fibers. Springer Series in Materials Science, vol. 210, Springer, Netherlands, 2015.
[25] S. Otani, Y. Fukuoka, B. Igarashi, K. Sasaki, Method for Producing Carbonized Lignin Fiber, U.S.P. Office, 1969. Nippon Kayaku Kk: US3461082 A.
[26] R.J. Moon, A. Martini, J. Nairn, J. Simonsen, J. Youngblood, Cellulose nanomaterials review: structure, properties and nanocomposites, Chem. Soc. Rev. 40 (7) (2011) 3941–3994.
[27] Y. Habibi, L.A. Lucia, O.J. Rojas, Cellulose nanocrystals: chemistry, self-assembly, and applications, Chem. Rev. 110 (6) (2010) 3479–3500.
[28] R.J. Moon, G.T. Schueneman, J. Simonsen, Overview of cellulose nanomaterials, their capabilities and applications, JOM 68 (9) (2016) 2383–2394.
[29] H. Chang, J. Luo, H.C. Liu, A.A.B. Davijani, P.-H. Wang, G.S. Lolov, R.M. Dwyer, S. Kumar, Ductile polyacrylonitrile fibers with high cellulose nanocrystals loading, Polymer 122 (2017) 332–339.
[30] H. Chang, A.-T. Chien, H.C. Liu, P.-H. Wang, B.A. Newcomb, S. Kumar, Gel spinning of polyacrylonitrile/cellulose nanocrystal composite fibers, ACS Biomater. Sci. Eng. 1 (7) (2015) 610–616.
[31] J. Luo, H. Chang, A.A.B. Davijani, H.C. Liu, P.-H. Wang, R.J. Moon, S. Kumar, Influence of high loading of cellulose nanocrystals in polyacrylonitrile composite films, Cellulose 24 (4) (2017) 1745–1758.
[32] S. Li, J. Lyons-Hart, J. Banyasz, K. Shafer, Real-time evolved gas analysis by FTIR method: an experimental study of cellulose pyrolysis, Fuel 80 (12) (2001) 1809–1817.
[33] Z. Bashir, A critical review of the stabilisation of polyacrylonitrile, Carbon 29 (8) (1991) 1081–1090.
[34] M.S.A. Rahaman, A.F. Ismail, A. Mustafa, A review of heat treatment on polyacrylonitrile fiber, Polym. Degrad. Stabil. 92 (8) (2007) 1421–1432.
[35] S. Allen, M. Fujii, V. Stannett, H. Hopfenberg, J. Williams, The barrier properties of polyacrylonitrile, J. Membr. Sci. 2 (1977) 153–163.
[36] G. Strupinsky, A.L. Brody, A twenty-year retrospective on plastics: oxygen barrier packaging materials, in: Polymers, Laminations & Coatings Conference Proceedings, 1998.
[37] Y. Liu, S. Kumar, Recent progress in fabrication, structure, and properties of carbon fibers, Polym. Rev. 52 (3) (2012) 234–258.
[38] M.-y. Lv, H.-y. Ge, J. Chen, Study on the chemical structure and skin-core structure of polyacrylonitrile-based fibers during stabilization, J. Polym. Res. 16 (5) (2009) 513–517.
[39] S. Belbekhouche, J. Bras, G. Siqueira, C. Chappey, L. Lebrun, B. Khelifi, S. Marais, A. Dufresne, Water sorption behavior and gas barrier properties of cellulose whiskers and microfibrils films, Carbohydr. Polym. 83 (4) (2011) 1740–1748.
[40] F. Li, P. Biagioni, M. Bollani, A. Maccagnan, L. Piergiovanni, Multi-functional coating of cellulose nanocrystals for flexible packaging applications, Cellulose 20 (5) (2013) 2491–2504.
[41] D.F. Arseneau, Competitive reactions in the thermal decomposition of cellulose, Can. J. Chem. 49 (4) (1971) 632–638.
[42] Y. Peng, D.J. Gardner, Y. Han, A. Kiziltas, Z. Cai, M.A. Tshabalala, Influence of drying method on the material properties of nanocellulose I: thermostability and crystallinity, Cellulose 20 (5) (2013) 2379–2392.
[43] N. Quiévy, N. Jacquet, M. Sclavons, C. Deroanne, M. Paquot, J. Devaux, Influence of homogenization and drying on the thermal stability of microfibrillated cellulose, Polym. Degrad. Stabil. 95 (3) (2010) 306–314.
[44] R. Mathur, O. Bahl, J. Mittal, A new approach to thermal stabilisation of PAN fibres, Carbon 30 (4) (1992) 657–663.
[45] D. Klemm, B. Philipp, T. Heinze, U. Heinze, W. Wagenknecht, Comprehensive Cellulose Chemistry Volume 1: Fundamentals and Analytical Methods, vol. 1, Wiley-VCH, Weinheim, 1998.
[46] M. Fan, D. Dai, B. Huang, Fourier Transform Infrared Spectroscopy for Natural Fibres. Fourier Transform–Materials Analysis, 2012, p. 48. https://www.intechopen.com/books/fourier-transform-materials-analysis/fourier-transform-infrared-spectroscopy-for-natural-fibres.
[47] A.D. French, Idealized powder diffraction patterns for cellulose polymorphs, Cellulose 21 (2) (2014) 885–896.
[48] A. Kumar, Y.S. Negi, V. Choudhary, N.K. Bhardwaj, Characterization of cellulose nanocrystals produced by acid-hydrolysis from sugarcane bagasse as agro-waste, J. Mater. Chem. Phys. 2 (1) (2014) 1–8.
[49] A. Gupta, R. Singhal, Effect of copolymerization and heat treatment on the structure and x-ray diffraction of polyacrylonitrile, J. Polym. Sci., Polym. Phys. Ed. 21 (11) (1983) 2243–2262.
[50] H.E. Kissinger, Reaction kinetics in differential thermal analysis, Anal. Chem. 29 (11) (1957) 1702–1706.
[51] C.R. Nair, K. Krishnan, K. Ninan, Differential scanning calorimetric study on the Claisen rearrangement and thermal polymerisation of diallyl ether of bisphenols, Thermochim. Acta 359 (1) (2000) 61–67.
[52] H. Yang, R. Yan, H. Chen, D.H. Lee, C. Zheng, Characteristics of hemicellulose, cellulose and lignin pyrolysis, Fuel 86 (12) (2007) 1781–1788.
[53] A.B. Reising, R.J. Moon, J.P. Youngblood, Effect of particle alignment on mechanical properties of neat cellulose nanocrystal films, J. Sci. Technol. For. Prod. Process. 2 (6) (2012) 32–41.